Condensable Vapor Sorption by Low Charge State Protein Ions

Jihyeon Lee,[1] Brian H. Clowers,[2] & Christopher J. Hogan[1*]

[1]Department of Mechanical Engineering, University of Minnesota, Minneapolis, MN, 55455, USA

[2]Department of Chemistry, Washington State University, Pullman, WA, 99164, USA

*To whom correspondence should be addressed: hogan108@umn.edu

ABSTRACT

Measurement of the gas-phase ion mobility of protein ions provides a means to quantitatively assess the relative sizes of charged proteins. However, protein ion mobility measurements are typically singular values. Here we apply tandem mobility analysis to low charge state protein ions (+1 and +2 ions) introduced into the gas phase by nanodroplet nebulization. We first determine protein ion mobilities in dry air, and subsequently examine shifts in mobilities brought about by the clustering of vapor molecules. Tandem mobility analysis yields mobility-vapor concentration curves for each protein ion, expanding the information obtained from mobility analysis. This experimental procedure and analysis is extended to bovine serum albumin, transferrin, immunoglobulin G, and apoferritin with water, 1-butanol, and nonane. All protein ions appear to adsorb vapor molecules, with mobility "diameter" shifts of up to 6-7% at conditions just below vapor saturation. We parameterize results using κ- Köhler theory, where the term κ quantifies the extent of uptake beyond Köhler model expectations. For 1-butanol and nonane, κ decreases with increasing protein ion size, while it increases with increasing protein ion size for water. For the systems probed, the extent of mobility shift for the organic vapors is unaffected by the nebulized solution pH, while shifts with water are sensitive to pH.

Keywords: Gas-Phase Ion Mobility; Nebulization; Tandem Ion Mobility; Differential Mobility Analysis; Proteins

INTRODUCTION

Ion mobility spectrometry (IMS)[1], either as a standalone technique or in conjunction with mass spectrometry,[2] facilitates characterization of the structures of protein ions; measured mobilities can be converted either to collision cross sections via the foundational relationships first noted by Langevin (i.e. Mason-Schamp equation)[3] or to mobility diameters via the Stokes-Millikan equation.[4-5] A number of IMS studies in the past two decades have shown that structural features for a number of proteins and protein multimers are maintained when charged species transition from the solution to the gas-phase[6-7] establishing the use of IMS as an essential characterization tool for protein structural biology.[8-9] However, a feature of the standard, low-field strength IMS experiment is that for a given ion (chemical composition and charge state), the measurement yields a single mobility value which is largely dependent on three properties of the ion and bath gas: (1) the ion overall "size", often scaling with molecular mass for protein ions;[10] (2) the ion charge state, not only because mobility is proportional to charge but because high levels of charge lead to Coulombic stretching in protein and macromolecular ions;[11-13] and (3) the polarizability of bath gas in which the measurement is made.[14-15] This limits IMS largely to global size characterization.

In field asymmetric waveform IMS and other variants of IMS where separation is not based purely upon mobility but instead upon differences in low field and high field mobilities for an ion, limitations in chemical selectivity have been overcome by introducing condensable vapor molecules alongside the IMS bath gas[16-21] (i.e. vapor molecules of compounds which would be in the liquid or solid state at the measurement conditions, hence the vapor molecules only comprise a small fraction of the bath gas). At these sub-saturated concentrations, condensable vapor molecules transiently and selectively bind to analyte ions. For low mass analytes in traditional

low-field IMS measurements, theories describing the transient binding of condensable species have also been developed[22-30] and compared to measurements; both theory and measurements show that the transient binding of condensable vapors shift experimental mobilities to smaller values.[31-32] Most importantly, the extent of the observed shift is dependent upon the binding free energy of the vapor to the ion and the vapor molecule size relative to the ion size. Several studies have also demonstrated that the presence of condensable organic vapor molecules in the bath gas during IMS measurements of protein ions (primarily cytochrome C as a model protein) yields shifts in ion mobilities which can be attributed primarily to condensable vapor binding[33-34]. However, these prior efforts focused largely on highly charged protein ions (i.e. the +7 charge state of cytochrome C or higher). Ignoring the impacts of solution ionization conditions, sufficiently highly charged protein ions are Coulombically stretched in the gas phase and in examining mobility shifts due to vapor clustering for highly charged protein ions, vapor binding may simultaneously alter the extent of Coulombic stretching and the ion size, complicating the interpretation of results.

Here, we examine protein ion mobility shifts in the presence of water, 1-butanol, and nonane at vapor concentrations up to saturation. As model systems we used bovine serum albumin (66kDa)[35], transferrin (79.5kDa)[36], immunoglobulin G (150kDa)[37], and apoferritin (444kDa)[38], with measurements in air at atmospheric pressure and 295 K. These measurement conditions not only enable assessment of protein ion specific levels of vapor uptake, but in the case of water are also relevant to conditions downstream of commonly employed electrospray ionization sources for protein ions. Measurements were carried out via tandem differential mobility analysis (TDMA),[39-41] an approach commonly used to examine vapor uptake and the hygroscopic behavior of aerosol nanoparticles.[42] Unique from prior vapor uptake assessments

for protein ions, protein ions were generated using a nanodroplet nebulizer[43-46] and atmospheric pressure chemical ionization, *in lieu* of an electrospray emitter. This approach produces only singly and doubly charged protein ions, reducing Coulombic stretching for the protein ions examined. We quantify the extent of vapor uptake by evaluating experimental trends in vapor with κ- Köhler theory,[47-48] which is commonly used to describe the potential for water uptake and cloud condensation nucleus activity in aerosols.

EXPERIMENTAL METHODS

Bovine serum albumin (A9647), transferrin (human, T8158), immunoglobulin G (human, 56834), and apoferritin (horse spleen, A3641) were purchased from Sigma Aldrich in powder form. 10-30 micrograms per milliliter of each protein were dissolved in ultra-pure water (UPW system, Smith Engineering, Inc.) and then diluted with UPW again dilution ratios from 23.3 – 140 prior to aerosolization and TDMA measurements (adjusted to ensure monomer proteins were detected in high abundance). To adjust pH levels, ammonium hydroxide solution (Arcros Organics) and formic acid solution (Honeywell) were added to the sample, and pH levels were confirmed by pH testing strips before measurements.

The mobility-based size distributions of protein ions were first measured in a manner similar to that described by a number of prior studies (i.e. using a single differential mobility analyzer (DMA)[49] coupled to a condensation particle counter (CPC)).[50-54] A schematic diagram of the specific system employed is shown in Figure S1a of the supporting information, along with a brief description of these measurements. Figure S1b of the supporting provides a schematic diagram of the system used for TDMA vapor uptake experiments. Traditionally DMA-CPC measurements of protein ions were performed using a charge reduction electrospray

source[55-57] to introduce singly and doubly charged protein ions into the gas phase. Here, a nanoaerosol generator (NAG, Kanomax FMT), which is a nebulizer designed to produce submicrometer droplets,[43-46] was instead employed to aerosolize proteins into the gas phase. In the NAG, the prepared sample solution of proteins was introduced to a pneumatic nebulizer, held at 241 kPa backing pressure, with the solution dispersed into droplets at a liquid flow rate less than 1.0 mL min^{-1} (though varied for different proteins). After evaporation of the droplets, facilitated by passing them through an evaporator at 80 °C, solvent-free proteins were carried out of the NAG with a clean gas flow of 1.0 L min^{-1}. A diffusion dryer installed downstream of the NAG further reduced humidity down to ~10%, measured previously using a chilled-mirror hygrometer (General eastern, Hygro M4)). The gas phase proteins are largely neutral in charge upon generation via the NAG. They were hence ionized by a Kr-85 radioactive source emitting beta rays, which ionize gas molecules bipolarly.[58] Passage of proteins through such radioactive sources facilitates their interaction with smaller mass ions. Through ion-protein collisions and subsequent charge transfer from ions to proteins, protein ions are generated. However, a distribution of charge states exists, wherein the majority of proteins are still neutral, but a detectable fraction is singly or doubly charged across both polarities (i.e. positively and negatively charged species). Although not directly measured for proteins, measurements for smaller polymer ions suggest the resulting species are ionized by protonation and deprotonation reactions.[58] After ionization, protein ions were separated by a nano-differential mobility analyzer (nano-DMA, TSI) based upon their ion mobilities. For separation, the nano-DMA was operated with a circulating sheath flowrate of 6 L min^{-1}, with 0.6 L min^{-1} of the gas phase protein-laden flow entering the DMA. The DMA applied voltage was stepped from 0 to 150 V

over 40 measurement points for all protein except apoferritin, where a voltage range from 0 to 300 V over 60 measurement points was applied.

To perform tandem ion mobility measurements the flow exiting the first DMA was then transmitted into a second DMA, which was operated with a non-recirculating sheath flow of air, with its flow diagram shown in Figure 1c of the supporting information. The incoming sheath flow was clean air at 5.5 L min $^{-1}$, controlled by a mass flow controller. The clean air flow, along with a volumetric flow of liquid (water, nonane, or 1-butanol) in the range of 50-200 μL min $^{-1}$ (liquid, controlled by a syringe pump) was supplied to a T-junction held at 50 °C. The liquid was introduced continuously as droplets by a fused silica capillary tubing with a 250 μm ID. For all liquids, the droplets rapidly evaporated in the heated T-junction, and vaporized molecules were then carried within the air flow into the second DMA. We measured dew points with the chilled-mirror hygrometer; the measured dew points agreed with the calculated dew points within $\pm$0.5 K. The variations of the resulting sheath flow rate due to the addition of vapor molecules are not negligible in such TDMA systems. Therefore, the flow was continuously monitored with laminar flow elements (i.e. via pressure drop measurements) both upstream and downstream of the DMA (in the sheath flow path). These measurements were used to adjust the mass flow controller rate of clean air to maintain the total sheath flow rate of 5.5 L min $^{-1}$ through the second DMA for all vapor introduction conditions. At the downstream of the DMA, after the laminar flow element, a second mass flow controller was connected to a vacuum source to maintain 5.5 L min $^{-1}$ sheath flow rate. Downstream of the T-junction, the temperature of the whole system was held at 22 °C (room temperature). With the first DMA operating at fixed voltage to select protein ions of a given charge state (singly or doubly charged and positively charged) and cluster number (typically monomers, but also dimers and trimers for bovine serum

albumin), the mobility distributions of the selected protein ions were first measured without vapor introduction in the second DMA to establish a baseline for vapor uptake comparison. The second DMA was operated by stepping the voltage in the range corresponding to ±20% of the mobility diameter of selected protein ions with 12-16 measurement stages. Downstream of the second DMA, transmitted protein ions were detected via a fast time response condensation particle counter (FCPC, Kanomax FMT)[59]. The vapor concentration was systematically varied in the second DMA sheath flow, with mobility distributions for each vapor concentration. In total, measurements were conducted for four different proteins, three different vapors, and three different pH levels over the course of nine days. On each day, measurements were limited to one vapor type and one pH level to minimize system contamination and the effects of any day-to-day variation on flow and vapor concentrations. The second DMA was flushed with clean, dry, air continuously overnight between measurement days.

The data obtained from the measurements are the counts by FCPC, converted directly to a number concentration, as a function of DMA voltage. The voltage, V can be converted into the mobility, Z_p using geometries of the DMA by equation (1),

$$Z_p = \frac{q_{sh}}{2\pi VL} \ln\left(\frac{r_2}{r_1}\right) \quad (1)$$

where q_{sh} is sheath flow rate, L is the length of the DMA, r_1 is inner radius, and r_2 is outer radius. To convert ion mobility in the transition regime (Knudsen number dependent regime)[5, 60] to a measure of protein ion "size", we apply the Stokes-Millikan equation:

$$Z_p = \frac{neC_c}{3\pi\mu(d_p + d_g)} \quad (2)$$

where n is charge state, e is charge of electron, C_c is slip correction factor , μ is viscosity, d_p is the mobility diameter (i.e. the spherical equivalent diameter for the protein ion under the

measurement conditions), and d_g is the effective gas molecule diameter (approximately 0.3 nm in air)[4, 61]. The slip correction factor is expressed as follows:[62]

$$C_c = 1 + \frac{2\lambda}{(d_p+d_g)}\left(1.257 + 0.4e^{-0.55\frac{(d_p+d_g)}{\lambda}}\right) \quad (3)$$

where λ is mean free path of the gas. Mobility diameter distributions were used to compute a volume-weighted mean diameter ($\bar{d}_p$) at each vapor saturation ratio. From these relationships the growth factor was determined by normalizing the volume-weighted mean diameter at each saturation ratio by the mean diameter without vapor introduction. It is worth noting that this analysis approach is much simpler than the technique commonly used in inverting TDMA data[63] wherein DMA transfer functions are accounted for and distributions in the extent of vapor uptake are determined. The simplified approach is employed here because (1) protein ions are single molecule ions, as opposed to the highly heterogeneous particles commonly examined via TDMA measurements, (2) the protein ion mobility distributions are arguably as narrow or more narrow than the transmission function of the DMA utilized,[64] and (3) as shown in the Results & Discussion section, vapor-facilitated mobility shifts do not appear to substantially broaden mobility distributions, as would be the case if the growth factor had a broad distribution. κ-Köhler theory is a tractable method to parameterize our experimental results, which requires a careful accounting of the saturation ratio, S, over a droplet in equilibrium with its surroundings and can be described as follows:[47]

$$S = a_w \exp\left(\frac{4\sigma M_w}{RT\rho\bar{d}_p}\right) \quad (4)$$

where a_w is the activity of the liquid in the droplet, σ is surface tension, M_w is molecular weight of the liquid, R is universal gas constant, T is temperature, ρ is density of the liquid. The parameter κ is determined from:

$$\frac{1}{a_w} = 1 + \kappa \frac{V_s}{V_w} \quad (5)$$

where V_s is the volume of the dry ion and V_w is the volume of liquid condensed. With the conversion from volumes to diameters, the saturation ratio can be expressed with κ as follows,

$$S = \frac{\bar{d}_p{}^3 - \bar{d}_{p,d}{}^3}{\bar{d}_p{}^3 - \bar{d}_{p,d}{}^3(1-\kappa)} \exp\left(\frac{4\sigma M_w}{RT\rho\bar{d}_p}\right) \quad (6)$$

where $\bar{d}_p$ is the volume-weighted mobility diameter at the saturation ratio in question, and $\bar{d}_{p,d}$ is the volume weighted mobility diameter in the absence of condensable vapor. We found κ for each protein with each vapor type via a linear regression as described in the supporting information, based upon rearrangement of equation (6).

RESULTS AND DISCUSSION

Figure 1 displays the mobility diameter distributions of 4 protein ions, generated from pH 7 solution in the absence of condensable vapor. For each protein, the highest peak corresponds to monomer ions except for bovine serum albumin, where the highest peak corresponds to dimer ions and the second highest peak corresponds to monomer ions. The peak location was consistent over all measurements and the mobility diameters of bovine serum albumin, transferrin, immunoglobulin G, and apoferritin were 6.2 nm, 7.0 nm, 8.2 nm and 12.0 nm respectively, in reasonable agreement with original measurements of Kaufman et al.[50] for bovine serum albumin (6.04 nm) and immunoglobulin G (8.13 nm). Measurements are further in good agreement with spectroscopic measurements. Luzzati et al.[65] observed the radius of gyration of 3.06 nm for bovine serum albumin at pH 5.3 using small angle X-ray scattering. Martel et al.[66] investigated the structure of human transferrin with small angle neutron scattering and the radius of the

gyration of transferrin is 3.025 nm. Kilar et al.[67] measured the radii of immunoglobulin G1 (6 nm) and G3 (4.9 nm) using small angle X-ray scattering. Fischbach and Anderegg investigated the structure of apoferritin using X-ray scattering and showed apoferritin has a hollow sphere with an outer radius of 6.1 nm.[68] Peaks corresponding to doubly charged monomers were also identified, as they have twice the mobility of singly charged monomers (leading to a smaller inferred mobility diameter with a singly charged assumption). Peaks corresponding to multimeric ions were also observed due to the possibility of that single droplet contains proteins more than one during the nebulization process within NAG. The simulation by Lee et al.[46] suggest that similar mobility diameter distributions to figure 1 a-b are obtained when highly concentrated monodisperse particles are generated by a NAG. The charge assignment of different peaks and cluster state (M: monomer, D: dimer, and T: Trimer) are labelled in figure 1. Overall, the NAG and atmospheric pressure chemical ionization approach appears to yield protein ions similar to that produced by charge reduction electrospray sources.[50-53]

Figures 2-5 display mobility diameter distributions (normalized) of the singly charged monomers from pH 7 solutions, with the introduction of 3 different condensable vapors. The saturation ratio on a percent basis, at 295 K, is noted for each displayed distribution. Prior to discussing results for each protein and vapor examined, we remark that in all instances, we observe an increase in mobility diameter (i.e. a decrease in ion mobility) in the presence of introduced condensable vapor. Mobility shifts could certainly be brought about by changes in gas phase ion structure, and without direct mass shift measurements, mobility measurements alone do not prove vapor uptake occurs. However, detectable shifts with the modest resolving power (<10) mobility analyzers utilized in our measurements are highly indicative of vapor sorption during measurement. This can be contrasted with observed mobility shifts for higher

charge state protein ions in the presence of condensable vapor molecules; for example Butcher et al[34], using higher resolution instrumentation, found that in the mobility distributions of higher charge state (+5 and higher) cytochrome C and myoglobin ions specific peaks appear upon introduction of vapor molecules, and such peaks do not always appear at smaller mobilities (i.e. larger sizes). As Coulombic stretching likely plays some role in highly charged protein ion structure, changes in the mobilities of higher charge state protein ions are presumably due to a combination of conformational changes and vapor sorption.

We therefore proceed to analyze and discuss results under the assumption that mobility shifts are brought about largely because of vapor sorption by proteins in the gas phase. With water vapor, bovine serum albumin ions displayed minimal growth via vapor uptake; however, immunoglobulin G, and apoferritin grew much more noticeably. Conversely, with nonane and 1-butanol introduced as condensable vapors, all protein ions displayed clear size shifts, indicative of vapor uptake. Figure 6 provides the growth factors of protein ions with different condensable vapors introduced as a function of the saturation ratio. Measurement error was minimized and a high level of repeatability was achieved in measurements by monitoring the sheath flow rates with pressure sensors and injecting vapors with gas tight syringes. In general, the highest growth factor was observed with nonane vapor introduction followed by 1-butanol and water. Exceptionally, apoferritin showed the highest growth factors with water vapor introduction followed by nonane and 1-butanol. With water vapor, the growth ratios of larger protein ions (i.e. those with larger monomer mobility diameters) were higher than the growth factors of smaller protein ions. However, with nonane and 1-butanol, the opposite tendency was observed; smaller protein ions presented higher growth factors.

In addition to growth factors, the average of number of vapor molecules adsorbed onto protein monomer ions were estimated, based on the shift in mean protein ion volume at each saturation ratio and estimating vapor molecule volume based on molecular weight and bulk density. Results are summarized in table 1. With 100% saturation water vapor, on average 304.8 molecules, 475.2 molecules, 932.9 molecules, and 5418.7 molecules were condensed on bovine serum albumin monomers, transferrin monomers, immunoglobulin G monomers, and apoferritin monomers, respectively. With 100% saturation nonane vapor, 79.2 molecules, 113.5 molecules, 190.4 molecules, and 478.4 molecules were condensed on bovine serum albumin monomers, transferrin monomers, immunoglobulin G monomers, and apoferritin monomers, respectively. Lastly, with 75% saturation 1-butanol, 141.7 molecules, 185.0 molecules, 279.5 molecules, and 595.7 molecules were condensed on bovine serum albumin monomers, transferrin monomers, immunoglobulin G monomers, and apoferritin monomers, respectively.

In κ-Köhler theory, an ion size effect is naturally present via the Kelvin-capillarity term (i.e. the increase in saturation ratio by a factor $\exp\left(\frac{4\sigma M_w}{RT\rho\bar{d}_p}\right)$). A consequence of this term is that based on the capillarity model, higher saturation ratios should be required to drive vapor uptake for smaller ions. However, this is only observed for water (the highest surface tension condensable vapor) in the present study. This suggests that there are protein-specific activity coefficients for the condensable vapors examined, parameterized by κ. Figure 7 displays κ from regression to measurements with singly charged monomer ions from pH solution. We remark that as shown in the supporting information, fits to determine κ (which are forced through the origin) are not highly linear as they commonly are when examining vapor uptake by salt or other solvent-soluble molecule-containing aerosol particles. Therefore, the inferred κ are best utilized qualitatively to examine differences in uptake between the Köhler model (incorporated the

Kelvin effect and Raoult's law, but with $\kappa = 1$). Larger κ reflects greater affinity for the condensable vapor introduced. As expected, based upon mobility shifts, κ values for nonane are higher than those for the other two vapor types. κ for nonane and 1-butanol decreases with protein ion size, and κ for water increases as the size of protein increases, indicating even for water there is a size effect beyond that predicted by the capillarity model.

We therefore conclude that condensable vapor uptake by low charge state protein ions displays additional information beyond that from mobility measurements in the absence of condensable vapor; however, we still observe correlations between the extent of uptake and protein ion size (though with different trends in κ with size for different condensable vapor molecules). A subsequent concern is whether the extent of uptake change with original solution pH and protein ion extent of clustering. Figure 8 displays the growth factors of protein monomers at different pH levels. The isoelectric points of bovine serum albumin, transferrin, immunoglobulin G, and apoferritin are pH 4.5-5.0, 6, 6.6-7.2 and, 4.8, respectively, indicating all examined proteins are positively charged at pH 3 and negatively charged at pH 10. While the solution pH and charge state in solution has no apparent bearing on protein ion charge state based on the aerosolization and ionization mechanism employed in the present study, it may have an influence on the gas phase structure of each ion. It is worthy to note that we did not observe apoferritin dissocation in the high and low pH solutions examined, though these pHs are close to the apoferritin stability limits. In Figure 8, larger standard deviations and variations of the growth factors were observed with water vapor introduction only, with differences with nonane and 1-butanol introduction undetectable. This indicates that water vapor uptake in the gas phase is altered by changes in protein solution phase structure, with some of these changes

presumably maintained in the gas phase; however, the overall influence is small, and solution pH does not appear to greatly affect the vapor uptake by protein ions in the gas phase.

The growth factors of singly charged monomers and doubly charged monomers of bovine serum albumin are plotted as a function of saturation ratio for test 3 condensable vapors in Figure 9a-c. Importantly, we recover the same growth factors for both charge states. We note that in calculating these growth ratios, n = 2 (doubly charged) serves as the input into the Stokes-Millikan equation. Different growth factors for different charge states would likely suggest issues with calibration or in the data analysis approach employed as Coulombic influences in both singly and doubly charged protein ions in the size range are not significant enough to influence vapor uptake (though it can have a substantial effect at higher charge levels, or the single nanometer scale).[69-71] Figure 9d-f displays the growth factors of multimers of bovine serum albumin. Multimeric ion growth factors show the same tendency as monomer ions; larger proteins grew more with water vapor and smaller proteins grew more with nonane and 1-butanol vapor, and the effect is small with bovine serum albumin. With water vapor, the multimer growth factors observed here are slightly below those observed for similar saturation ratios by Wang et al., who examined 40 nm -100 nm larger protein particles.[72] However, because of the observed size dependency of water uptake, we find our results are consistent with this prior study.

By examining bovine serum albumin multimer growth factors alongside other proteins, we find that the water growth factor is not solely determined by protein ion mobility diameter but also dependent upon the protein itself. As shown in Figure 10, for different water vapor saturation ratios, the growth factors of multimers of albumin protein ions are smaller than growth factors of transferrin and immunoglobulin G, even when mobility diameters of multimers are

larger than those of transferrin and immunoglobulin G monomers. Meanwhile, with nonane vapor and 1-butanol vapor, the size of the protein ion likely plays a more dominant role in determining extent of vapor uptake, as the growth ratios mostly agree well with the order of mobility diameters of protein ions, irrespectively of exact protein composition.

CONCLUSIONS

We examined the condensable-vapor induced mobility shifts of four protein ions in the mass range of 66-444 kDa by tandem DMA measurements, using three different condensable vapors with protein ions produced from three different pH level solutions. Results reveal consistent decreases in mobility with increasing condensable-vapor concentrations, which we interpret as strong evidence for subsaturated vapor uptake by protein ions. To avoid Coulombic stretching of resulting protein ions which occurs at sufficiently high charge state, ions were generated first using pneumatic nebulizer for aerosolization and second using Kr-85 radioactive source for atmospheric pressure chemical ionization, yielding only singly and doubly charged protein ions. The mobility diameters of protein ions, determined using the Stokes-Millikan equation, are comparable to those produced by charge reduction electrospray sources. For monomers generated from pH 7 solution, the growth factors with water vapor increased as the size of protein increases. This trend with size however is reversed with nonane and 1-butanol; for these condensable vapors the growth factor decreased with increasing ion mobility diameter. The introduction of nonane vapor yielded the highest growth factors, around 1.06 at saturation, for bovine serum albumin, transferrin, and immunoglobulin G ions, whereas apoferritin ions grew

most noticeably with water vapor. Fitting to κ – Köhler theory, κ values for nonane were higher than for 1-butanol and water. Changes in pH of the original protein solution did not lead to appreciable impacts on growth factors. Additionally, we observed that the growth factors of singly and doubly charged bovine serum albumin ions are identical. Multimer ion growth factors show the same tendency as monomer ions.

In total, measurements demonstrate how controlled condensable vapor introduction yields additional information from mobility measurements beyond the information from traditional low-field IMS experiments. At the same time, much of the observed mobility shift behavior can be correlated with mobility diameter, suggesting vapor-induced mobility modulation for protein ions is not completely orthogonal as a separation or characterization approach to standard mobility measurement. Nonetheless, we argue that modulation of condensable vapor concentrations may be a useful tool in optimizing mobility based measurement schemes, not only for small ions as examined in previous work,[24, 29-30] but also macromolecular ions. Controlled condensation of vapors onto ions likely also impacts ion reactivity in the vapor phase (e.g. products of collision induced dissociation for multiprotein complexes[73]) and may further be exploited in the development of tandem mobility-mass spectrometry measurement schemes.

SUPPORTING INFORMATION

Schematic diagrams of the measurement systems utilized, details on single DMA-CPC measurements, and details on data analysis via κ- Köhler theory are available online.

ACKNOWLEDGEMENTS

This work was supported by US National Science Foundation Awards 2002852 and 2003042.

Table 1. Nominal number of vapor molecules condensed on protein monomer ions generated from pH 7 solution at each saturation ratio.

Vapor	Water		Nonane				1-Butanol		
Saturation ratio (%)	**50%**	**100%**	**25%**	**50%**	**75%**	**100%**	**25%**	**50%**	**75%**
Bovine serum albumin	80.7	304.8	20.1	42.8	64.6	79.2	62.5	94.5	141.7
Transferrin	174.8	475.2	29.0	61.8	94.5	113.5	95.8	139.9	185.0
Immunoglobulin G	343.8	932.9	50.8	100.1	163.1	190.4	137.6	202.1	279.5
Apoferritin	1614.1	5418.7	117.1	239.1	404.2	478.4	306.7	423.5	595.7

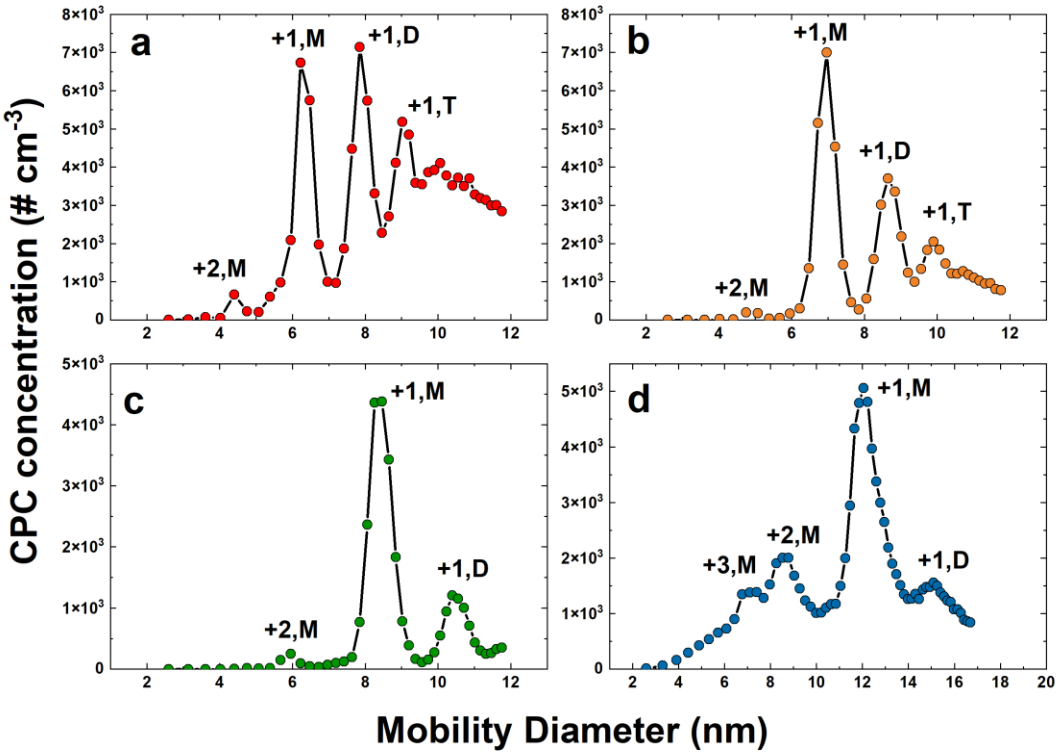

Figure 1. Mobility diameter distributions of all proteins in air nebulized at a pH of 7. (**a)** Bovine serum albumin. (**b)** Transferrin. (**c)** Immunoglobulin G. (**d)** Apoferritin. +1 and +2 indicate the charge state, while M, D, and T indicate monomers, dimers, and trimers respectively.

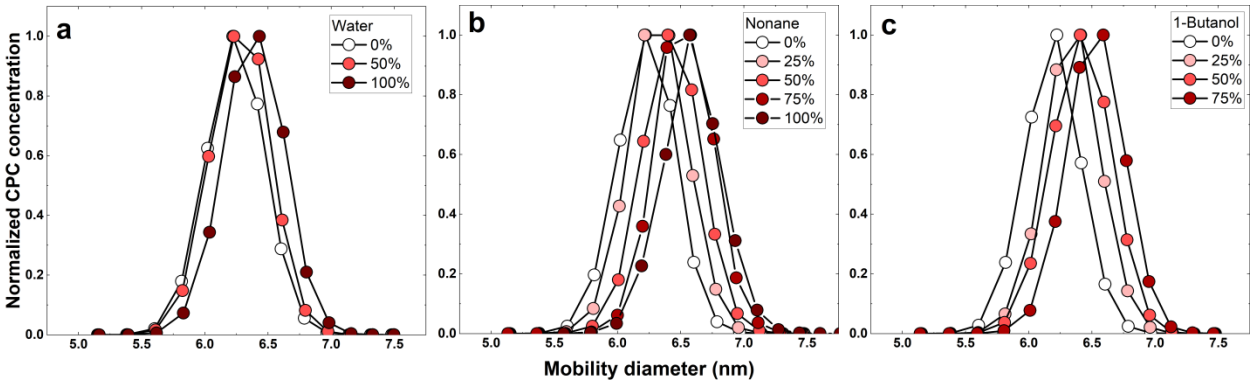

Figure 2. Mobility diameter distributions of singly charged bovine serum albumin monomers with **(a)** water introduction, **(b)** nonane introduction, and **(c)** 1-butanol introduction.

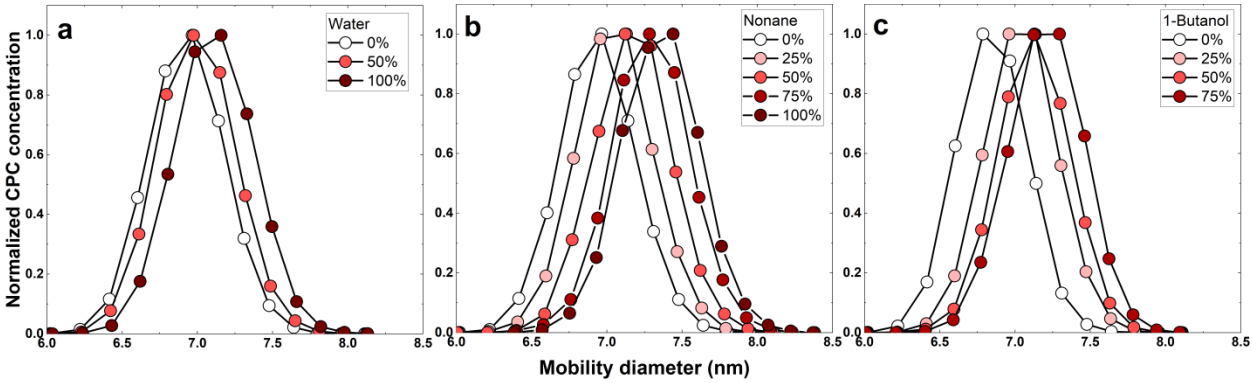

Figure 3. Mobility diameter distributions of singly charged transferrin monomers with **(a)** water introduction, **(b)** nonane introduction, and **(c)** 1-butanol introduction.

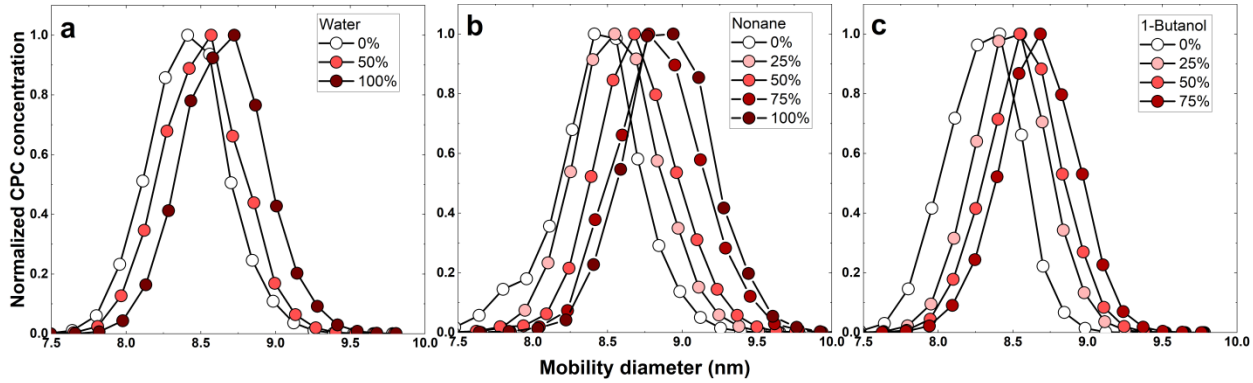

Figure 4. Mobility diameter distributions of singly charged immunoglobulin G monomers with **(a)** water vapor introduction, **(b)** nonane introduction, and **(c)** 1-butanol introduction.

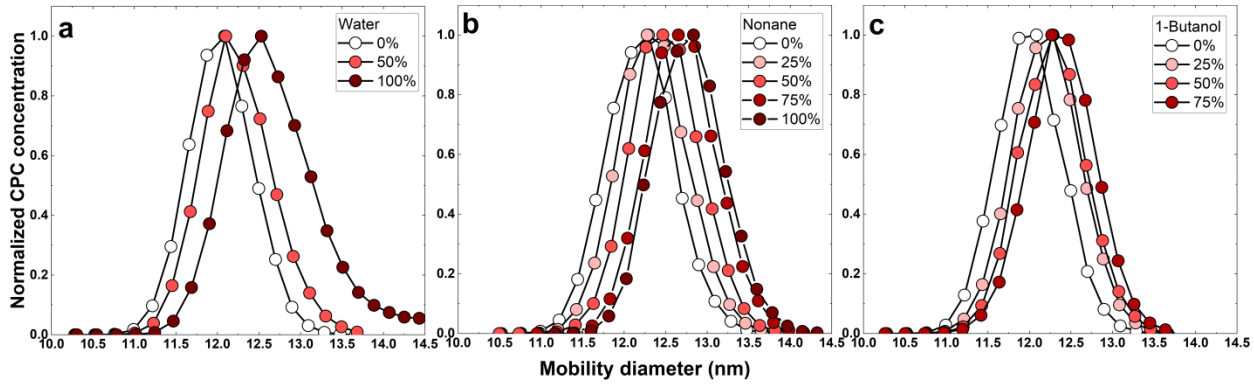

Figure 5. Mobility diameter distributions of singly charged apoferritin monomers with **(a)** water introduction, **(b)** nonane introduction, and **(c)** 1-butanol introduction.

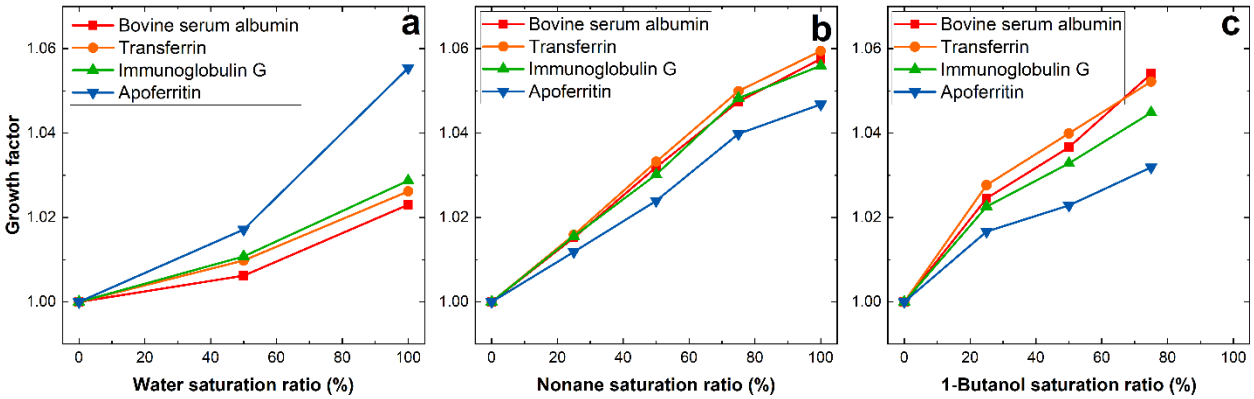

Figure 6. Growth factors of monomers with **(a)** water introduction, **(b)** nonane introduction, and **(c)** 1-butanol introduction.

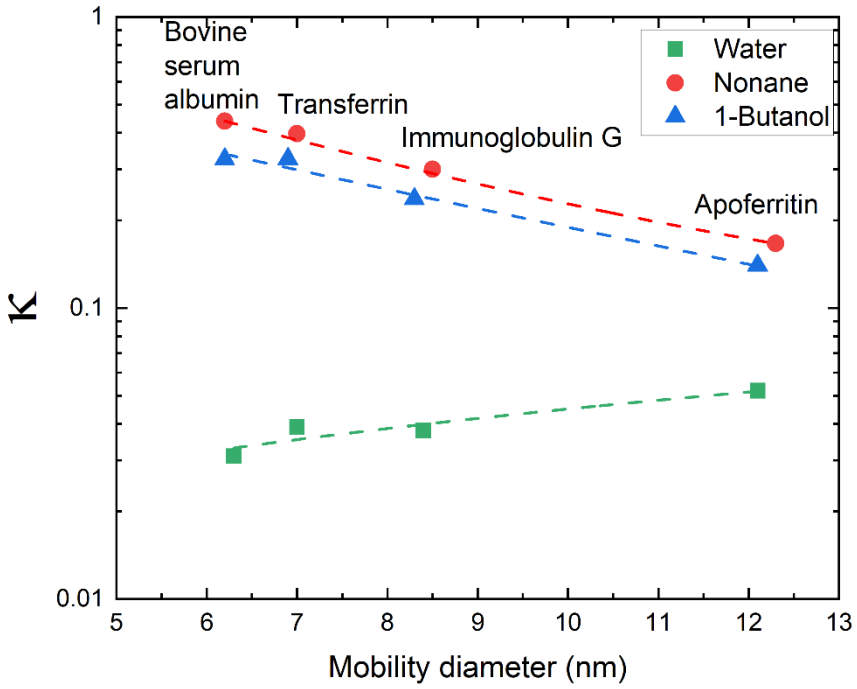

Figure 7. Inferred κ of protein monomers for each condensable vapor.

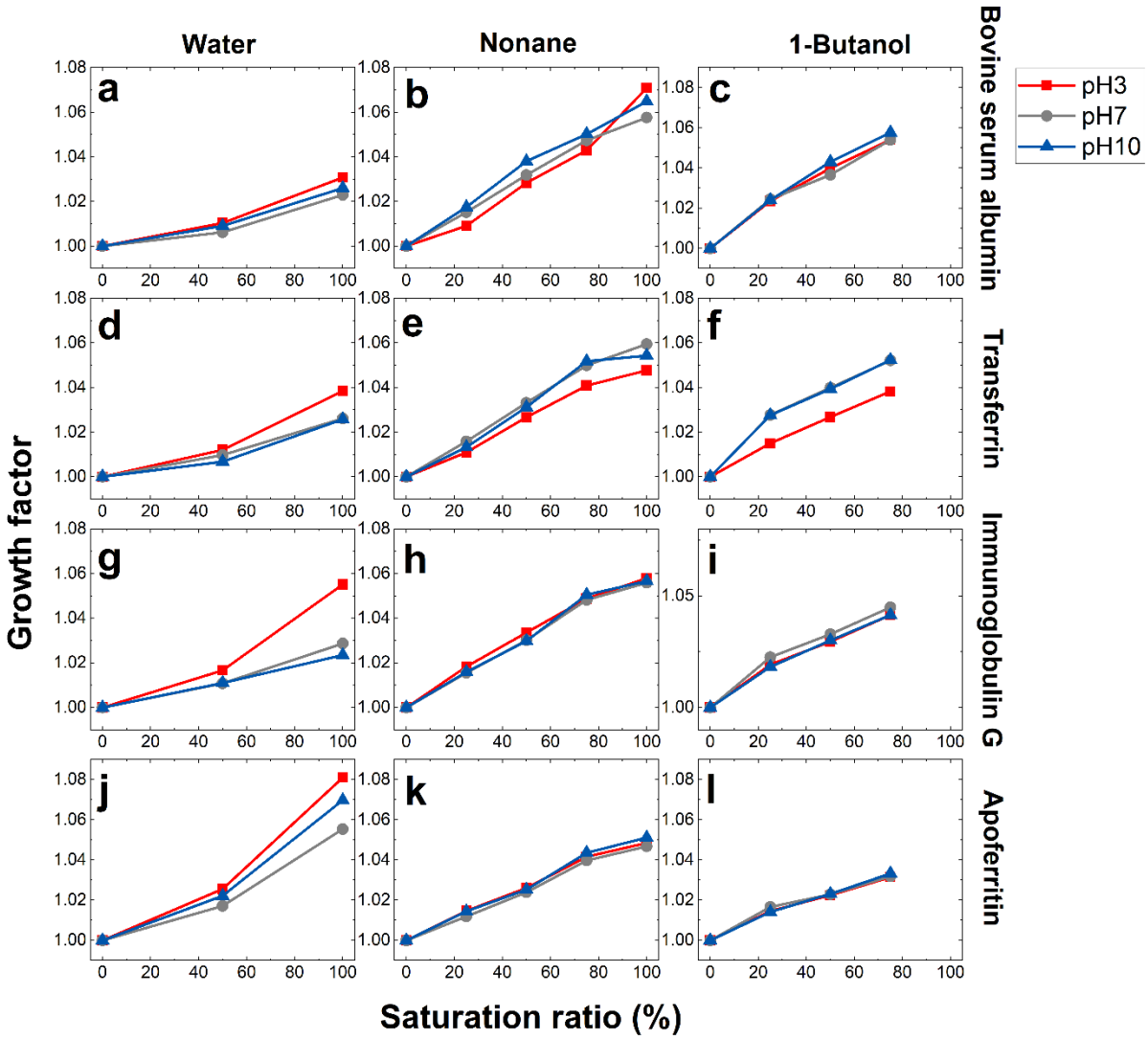

Figure 8. The growth factors of proteins exposed to condensable vapors nebulized at different pH levels. **a)** bovine serum albumin – water, **b)** bovine serum albumin – nonane, **c)** bovine serum albumin – 1-butanol, **d)** transferrin – water, **e)** transferrin – nonane, **f)** transferrin – 1-butanol, **g)** immunoglobulin G – water, **h)** immunoglobulin G -nonane, **i)** immunoglobulin G – 1-butanol, **j)** apoferritin – water, **k)** apoferritin – nonane and **l)** apoferritin – 1-butanol

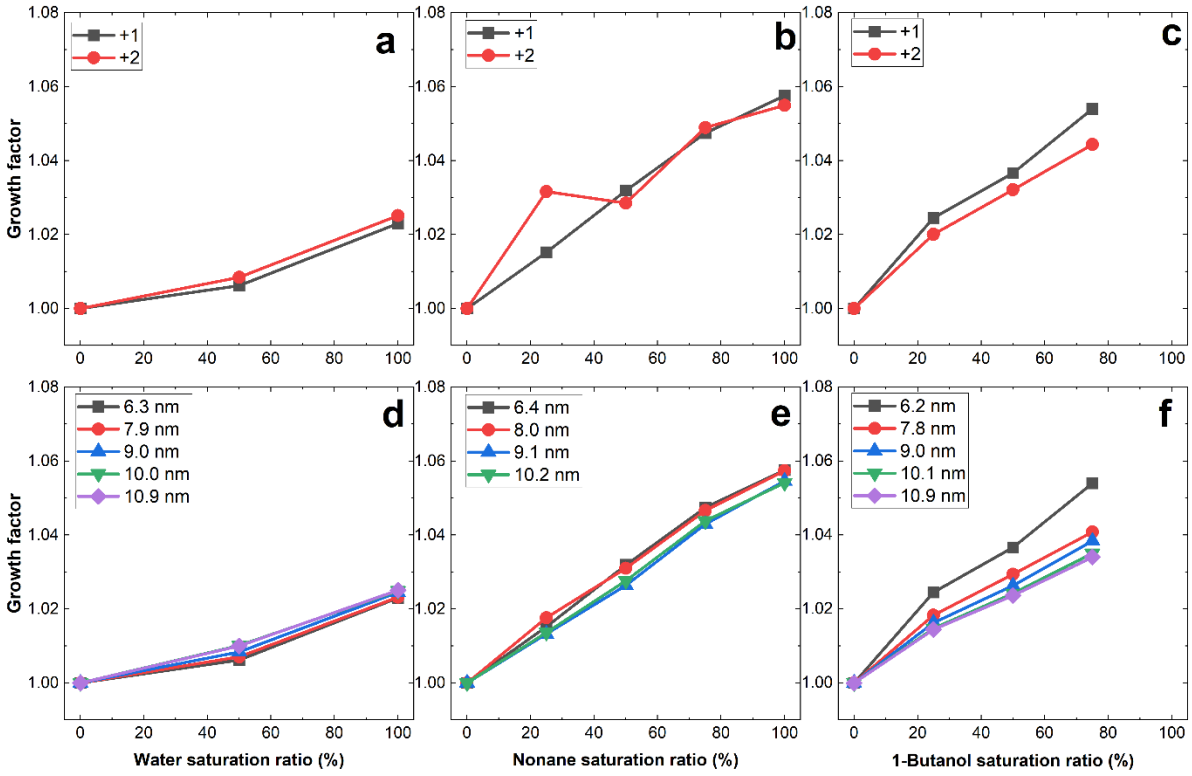

Figure 9. Growth factors of doubly and singly charged bovine serum albumin monomers with **(a)** water introduction, **(b)** nonane introduction, and **(c)** 1-butanol introduction. Growth factors of bovine serum albumin multimers with **(d)** water introduction **(e)** nonane introduction **(f)** 1-butanol introduction.

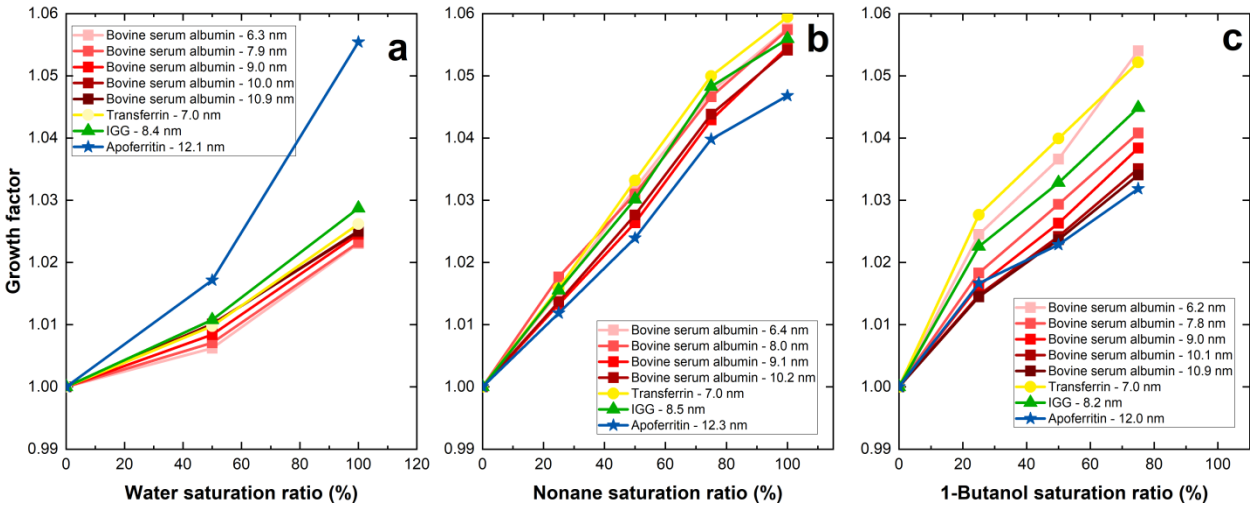

Figure 10. Growth factors of different protein ions including multimers of bovine serum albumin protein ions with **(a)** water introduction, **(b)** nonane introduction, and **(c)** 1-butanol introduction.

References

1. Revercomb, H. E.; Mason, E. A. Theory of Plasma Chromatography Gaseous Electrophoresis - Review. *Anal. Chem.* **1975,** *47* (7), 970-983.
2. Bohrer, B. C.; Merenbloom, S. I.; Koeniger, S. L.; Hilderbrand, A. E.; Clemmer, D. E. Biomolecule Analysis by Ion Mobility Spectrometry. *Ann. Rev. Anal. Chem.* **2008,** *1*, 293-327.
3. McDaniel, E. W.; Mason, E. A. *The Mobility and Diffusion of Ions in Gases*. 1973.
4. Larriba, C.; Hogan, C. J.; Attoui, M.; Borrajo, R.; Fernandez-Garcia, J.; Fernandez de la Mora, J. The Mobility-Volume Relationship below 3.0 nm examined by Tandem Mobility-Mass Measurement. *Aerosol Sci. Technol.* **2011,** *45*, 453-467.
5. Larriba-Andaluz, C.; Carbone, F. The size-mobility relationship of ions, aerosols, and other charged particle matter. *J. Aerosol Sci.* **2021,** *151*, 105659.
6. Ruotolo, B. T.; Giles, K.; Campuzano, I.; Sandercock, A. M.; Bateman, R. H.; Robinson, C. V. Evidence for macromolecular protein rings in the absence of bulk water. *Science* **2005,** *310*, 1658-1661.
7. Ruotolo, B. T.; Robinson, C. V. Aspects of native proteins are retained in vacuum. *Curr. Op. Chem. Biol.* **2006,** *10* (5), 402-408.
8. Ruotolo, B. T.; Benesch, J. L. P.; Sandercock, A. M.; Hyung, S. J.; Robinson, C. V. Ion mobility-mass spectrometry analysis of large protein complexes. *Nature Protocols* **2008,** *3* (7), 1139-1152.
9. Ben-Nissan, G.; Sharon, M. The application of ion-mobility mass spectrometry for structure/function investigation of protein complexes. *Curr. Op. Chem. Biol.* **2018,** *42*, 25-33.
10. Bush, M. F.; Hall, Z.; Giles, K.; Hoyes, J.; Robinson, C. V.; Ruotolo, B. T. Collision Cross Sections of Proteins and their Complexes: a Calibration Framework and Database for Gas-Phase Structural Biology. *Anal. Chem.* **2010,** *82*, 9557-9565.
11. Larriba, C.; Fernandez de la Mora, J. The Gas Phase Structure of Coulombically Stretched Polyethylene Glycol Ions. *J. Phys. Chem. B* **2012,** *116*, 593-598.
12. González Flórez, A. I.; Mucha, E.; Ahn, D.-S.; Gewinner, S.; Schöllkopf, W.; Pagel, K.; von Helden, G. Charge-Induced Unzipping of Isolated Proteins to a Defined Secondary Structure. *Angewandte Chemie Int. Ed.* **2016,** *55* (10), 3295-3299.
13. Abramsson, M. L.; Sahin, C.; Hopper, J. T. S.; Branca, R. M. M.; Danielsson, J.; Xu, M.; Chandler, S. A.; Österlund, N.; Ilag, L. L.; Leppert, A., et al. Charge Engineering Reveals the Roles of Ionizable Side Chains in Electrospray Ionization Mass Spectrometry. *JACS Au* **2021,** *1* (12), 2385-2393.
14. Naylor, C. N.; Reinecke, T.; Clowers, B. H. Assessing the Impact of Drift Gas Polarizability in Polyatomic Ion Mobility Experiments. *Anal. Chem.* **2020,** *92* (6), 4226-4234.
15. Asbury, G. R.; Hill, H. H. Using Different Drift Gases To Change Separation Factors (α) in Ion Mobility Spectrometry. *Anal. Chem.* **2000,** *72* (3), 580-584.
16. Waraksa, E.; Perycz, U.; Namieśnik, J.; Sillanpää, M.; Dymerski, T.; Wójtowicz, M.; Puton, J. Dopants and gas modifiers in ion mobility spectrometry. *TrAC Trends Anal. Chem.* **2016,** *82*, 237-249.
17. Rorrer, L. C.; Yost, R. A. Solvent vapor effects on planar high-field asymmetric waveform ion mobility spectrometry. *Int. J. Mass Spectrom.* **2011,** *300* (2), 173-181.
18. Schneider, B. B.; Covey, T. R.; Nazarov, E. G. DMS-MS separations with different transport gas modifiers. *Int. J. Ion Mobility Spectrom.* **2013,** *16* (3), 207-216.

19. Purves, R. W.; Ozog, A. R.; Ambrose, S. J.; Prasad, S.; Belford, M.; Dunyach, J.-J. Using Gas Modifiers to Significantly Improve Sensitivity and Selectivity in a Cylindrical FAIMS Device. *J. Amer. Soc. Mass Spectrom.* **2014,** *25* (7), 1274-1284.
20. Kafle, A.; Coy, S. L.; Wong, B. M.; Fornace, A. J.; Glick, J. J.; Vouros, P. Understanding Gas Phase Modifier Interactions in Rapid Analysis by Differential Mobility-Tandem Mass Spectrometry. *J. Amer. Soc. Mass Spectrom.* **2014,** *25* (7), 1098-1113.
21. Rorrer, L. C.; Yost, R. A. Solvent vapor effects in planar high-field asymmetric waveform ion mobility spectrometry: Solvent trends and temperature effects. *Int. J. Mass Spectrom.* **2015,** *378*, 336-346.
22. Maisser, A.; Hogan, C. J. Examination of Organic Vapor Adsorption onto Alkali Metal and Halide Atomic Ions via Ion Mobility-Mass Spectrometry. *ChemPhysChem* **2017,** *18*, 3039-3046.
23. Thomas, J. M.; He, S.; Larriba-Andaluz, C.; DePalma, J. W.; Johnston, M. V.; Hogan, C. J. Ion Mobility Spectrometry-Mass Spectrometry Examination of the Structures, Stability, and Extent of Hydration of Dimethylamine-Sulfuric Acid Clusters. *Phys. Chem. Chem. Phys.* **2016,** *18*, 22962-22972
24. Kwantwi-Barima, P.; Ouyang, H.; Hogan, C. J.; Clowers, B. H. Tuning Mobility Separation Factors of Chemical Warfare Agent Degradation Products via Selective Ion-Neutral Clustering. *Anal. Chem.* **2017,** *89* (22), 12416-12424.
25. Li, C.; Hogan, C. J. Vapor specific extents of uptake by nanometer scale charged particles. *Aerosol Sci. Technol.* **2017,** *51* (5), 653-664.
26. Oberreit, D. R.; Rawat, V. K.; Larriba-Andaluz, C.; Ouyang, H.; McMurry, P. H.; Hogan, C. J. Analysis of heterogeneous water vapor uptake by metal iodide cluster ions via differential mobility analysis-mass spectrometry. *J. Chem. Phys.* **2015,** *143*, 104204.
27. Rawat, V. K.; Vidal-de-Miguel, G.; Hogan, C. J. Modeling vapor uptake induced mobility shifts in peptide ions observed with transversal modulation ion mobility spectrometry-mass spectrometry. *Analyst* **2015,** *140* (20), 6945-6954.
28. Ahonen, L.; Li, C.; Kubečka, J.; Iyer, S.; Vehkamäki, H.; Petäjä, T.; Kulmala, M.; Hogan Jr, C. J. Ion Mobility-Mass Spectrometry of Iodine Pentoxide–Iodic Acid Hybrid Cluster Anions in Dry and Humidified Atmospheres. *J. Phys. Chem. Lett.* **2019,** *10* (8), 1935-1941.
29. Kwantwi-Barima, P.; Hogan, C. J.; Clowers, B. H. Deducing Proton-Bound Heterodimer Association Energies from Shifts in Ion Mobility Arrival Time Distributions. *J. Phys. Chem. A* **2019,** *123* (13), 2957-2965.
30. Kwantwi-Barima, P.; Hogan, C. J.; Clowers, B. H. Probing Gas-Phase-Clustering Thermodynamics with Ion Mobility–Mass Spectrometry: Association Energies of Phenylalanine Ions with Gas-Phase Alcohols. *J. Amer. Soc. Mass Spectrom.* **2020,** *31* (9), 1803-1814.
31. Fernandez Maestre, R. Calibration of the mobility scale in ion mobility spectrometry: the use of 2,4-lutidine as a chemical standard, the two-standard calibration method and the incorrect use of drift tube temperature for calibration. *Anal. Methods* **2017,** *9* (29), 4288-4292.
32. Fernández-Maestre, R.; Meza-Morelos, D.; Wu, C. Shift reagents in ion mobility spectrometry: the effect of the number of interaction sites, size and interaction energies on the mobilities of valinol and ethanolamine. *J. Mass Spectrom.* **2016,** *51* (5), 378-383.
33. Meyer, N. A.; Root, K.; Zenobi, R.; Vidal-de-Miguel, G. Gas-Phase Dopant-Induced Conformational Changes Monitored with Transversal Modulation Ion Mobility Spectrometry. *Anal. Chem.* **2016,** *88* (4), 2033-2040.

34. Butcher, D.; Miksovska, J.; Ridgeway, M. E.; Park, M. A.; Fernandez-Lima, F. The effects of solution additives and gas-phase modifiers on the molecular environment and conformational space of common heme proteins. *Rapid Comm. Mass Spectrom.* **2019,** *33* (5), 399-404.
35. Hirayama, K.; Akashi, S.; Furuya, M.; Fukuhara, K.-i. Rapid confirmation and revision of the primary structure of bovine serum albumin by ESIMS and Frit-FAB LC/MS. *Biochem. Biophys Res. Comm.* **1990,** *173* (2), 639-646.
36. Roberts, R. C.; Makey, D. G.; Seal, U. S. Human transferrin: molecular weight and sedimentation properties. *J. Biol. Chem.* **1966,** *241* (21), 4907-4913.
37. Lambin, P. Reliability of molecular weight determination of proteins by polyacrylamide gradient gel electrophoresis in the presence of sodium dodecyl sulfate. *Anal. Biochem.* **1978,** *85* (1), 114-125.
38. Harrison, P. In *Ferritin: an iron-storage molecule*, Seminars in hematology, 1977; pp 55-70.
39. Rader, D. J.; McMurry, P. H. Application of the tandem differential mobility analyzer to studies of droplet growth or evaporation. *J. Aerosol Sci.* **1986,** *17* (5), 771-787.
40. Park, K.; Dutcher, D.; Emery, M.; Pagels, J.; Sakurai, H.; Scheckman, J.; Qian, S.; Stolzenburg, M. R.; Wang, X.; Yang, J., et al. Tandem Measurements of Aerosol Properties—A Review of Mobility Techniques with Extensions. *Aerosol Sci. Technol.* **2008,** *42* (10), 801-816.
41. Hämeri, K.; Väkevä, M.; Hansson, H.-C.; Laaksonen, A. Hygroscopic growth of ultrafine ammonium sulphate aerosol measured using an ultrafine tandem differential mobility analyzer. *J. Geophys.Res.: Atmospheres* **2000,** *105* (D17), 22231-22242.
42. Biskos, G.; Malinowski, A.; Russell, L. M.; Buseck, P. R.; Martin, S. T. Nanosize effect on the deliquescence and the efflorescence of sodium chloride particles. *Aerosol Sci. Technol.* **2006,** *40* (2), 97-106.
43. Jeon, S.; Oberreit, D. R.; Van Schooneveld, G.; Hogan, C. J. Nanomaterial size distribution analysis via liquid nebulization coupled with ion mobility spectrometry (LN-IMS). *Analyst* **2016,** *141* (4), 1363-1375.
44. Jeon, S.; Oberreit, D. R.; Van Schooneveld, G.; Hogan, C. J. Liquid Nebulization–Ion Mobility Spectrometry Based Quantification of Nanoparticle–Protein Conjugate Formation. *Anal. Chem.* **2016,** *88* (15), 7667-7674.
45. Jeon, S.; Oberreit, D. R.; Van Schooneveld, G.; Gao, Z.; Bischof, J. C.; Haynes, C. L.; Hogan, C. J. Ion-Mobility-Based Quantification of Surface-Coating-Dependent Binding of Serum Albumin to Superparamagnetic Iron Oxide Nanoparticles. *ACS Appl. Mat. Interfaces* **2016,** *8* (37), 24482-24490.
46. Lee, J.; He, S.; Song, G.; Hogan, C. J. Size distribution monitoring for chemical mechanical polishing slurries: An intercomparison of electron microscopy, dynamic light scattering, and differential mobility analysis. *Powder Technol.* **2022,** *396*, 395-405.
47. Petters, M. D.; Kreidenweis, S. M. A single parameter representation of hygroscopic growth and cloud condensation nucleus activity. *Atmos. Chem. Phys.* **2007,** *7* (8), 1961-1971.
48. Chang, R. Y. W.; Slowik, J. G.; Shantz, N. C.; Vlasenko, A.; Liggio, J.; Sjostedt, S. J.; Leaitch, W. R.; Abbatt, J. P. D. The hygroscopicity parameter (κ) of ambient organic aerosol at a field site subject to biogenic and anthropogenic influences: relationship to degree of aerosol oxidation. *Atmos. Chem. Phys.* **2010,** *10* (11), 5047-5064.
49. Knutson, E. O.; Whitby, K. T. Aerosol classification by electric mobility: apparatus, theory, and applications. *J. Aerosol Sci.* **1975,** *6* (6), 443-451.

50. Kaufman, S. L.; Skogen, J. W.; Dorman, F. D.; Zarrin, F.; Lewis, K. C. Macromolecule analysis based on electrophoretic mobility in air: Globular proteins. *Anal. Chem.* **1996,** *68* (11), 1895-1904.
51. Bacher, G.; Szymanski, W. W.; Kaufman, S. L.; Zöllner, P.; Blaas, D.; Allmaier, G. Charge-reduced nano electrospray ionization combined with differential mobility analysis of peptides, proteins, glycoproteins, noncovalent protein complexes and viruses. *J. Mass Spectrom.* **2001,** *36* (9), 1038-1052.
52. Kaddis, C. S.; Lomeli, S. H.; Yin, S.; Berhane, B.; Apostol, M. I.; Kickhoefer, V. A.; Rome, L. H.; Loo, J. A. Sizing Large Proteins and Protein Complexes by Electrospray Ionization Mass Spectrometry and Ion Mobility. *J. Amer. Soc. Mass Spectrom.* **2007,** *18* (7), 1206-1216.
53. Maiber, A.; Premnath, V.; Ghosh, A.; Nguyen, T. A.; Attoui, M.; Hogan, C. J. Determination of gas phase protein ion densities via ion mobility analysis with charge reduction. *Phys. Chem. Chem. Phys.* **2011,** *13* (48), 21630-21641.
54. Stolzenburg, M. R.; Mcmurry, P. H. An Ultrafine Aerosol Condensation Nucleus Counter. *Aerosol Sci. Technol.* **1991,** *14* (1), 48-65.
55. Scalf, M.; Westphall Michael, S.; Krause, J.; Kaufman Stanley, L.; Smith Lloyd, M. Controlling Charge States of Large Ions. *Science* **1999,** *283* (5399), 194-197.
56. Scalf, M.; Westphall, M. S.; Smith, L. M. Charge Reduction Electrospray Mass Spectrometry. *Anal. Chem.* **2000,** *72* (1), 52-60.
57. Tamadate, T.; Higashi, H.; Hogan, C. J.; Seto, T. The charge reduction rate for multiply charged polymer ions via ion–ion recombination at atmospheric pressure. *Phys. Chem. Chem. Phys.* **2020,** *22* (43), 25215-25226.
58. Maisser, A.; Thomas, J. M.; Larriba-Andaluz, C.; He, S.; Hogan, C. J. The Mass-Mobility Distributions of Ions Produced by a Po-210 Source in Air. *J. Aerosol Sci.* **2015,** *90*, 36-50.
59. Liu, Y.; Attoui, M.; Li, Y.; Chen, J.; Li, Q.; Wang, L. Characterization of a Kanomax® fast condensation particle counter in the sub-10 nm range. *J. Aerosol Sci.* **2021,** *155*, 105772.
60. Zhang, C.; Thajudeen, T.; Larriba, C.; Schwartzentruber, T. E.; Hogan, C. J. Determination of the Scalar Friction Factor for Non-spherical Particles and Aggregates Across the Entire Knudsen Number Range by Direct Simulation Monte Carlo (DSMC). *Aerosol Sci. Technol.* **2012,** *46*, 1065-1078.
61. Fernández-García, J.; Fernández de la Mora, J. Measuring the Effect of Ion-Induced Drift-Gas Polarization on the Electrical Mobilities of Multiply-Charged Ionic Liquid Nanodrops in Air. *J. Amer. Soc. Mass Spectrom.* **2013,** *24* (12), 1872-1889.
62. Davies, C. N. Definitive equations for the fluid resistance of spheres. *Proc. Phys. Soc.* **1945,** *57*, 259-270.
63. Gysel, M.; McFiggans, G. B.; Coe, H. Inversion of tandem differential mobility analyser (TDMA) measurements. *J. Aerosol Sci.* **2009,** *40* (2), 134-151.
64. You, R.; Li, M.; Guha, S.; Mulholland, G. W.; Zachariah, M. R. Bionanoparticles as Candidate Reference Materials for Mobility Analysis of Nanoparticles. *Anal. Chem.* **2014,** *86* (14), 6836-6842.
65. Luzzati, V.; Witz, J.; Nicolaieff, A. La structure de la sérum albumine de boeuf en solution à pH 5,3 et 3,6: Étude par diffusion centrale absolue des rayons X. *J. Molec. Biol.* **1961,** *3* (4), 379-392.
66. Martel, P.; Kim, S.; Powell, B. Physical characteristics of human transferrin from small angle neutron scattering. *Biophys. J.* **1980,** *31* (3), 371-380.

67. Kilár, F.; SIMONSimon, I.; Lakatos, S.; Vondervizt, F.; Medgyesi, G. A.; Závodszky, P. Conformation of human IgG subclasses in solution: Small-angle X-ray scattering and hydrodynamic studies. *Euro. J. Biochem.* **1985,** *147* (1), 17-25.
68. Fischbach, F.; Anderegg, J. An X-ray scattering study of ferritin and apoferritin. *J. Molecular Biol.* **1965,** *14* (2), 458-IN15.
69. Nasibulin, A. G.; Fernandez de la Mora, J.; Kauppinen, E. I. Ion-Induced Nucleation of Dibutyl Phthalate Vapors on Spherical and Nonspherical Singly and Multiply Charged Polyethylene Glycol Ions. *J. Phys. Chem. A* **2008,** *112* (6), 1133-1138.
70. Gamero-Castaño, M.; de la Mora, J. F. Ion-induced nucleation: Measurement of the effect of embryo's size and charge state on the critical supersaturation. *J. Chem. Phys* **2002,** *117* (7), 3345-3353.
71. Kuldinow, D.; Przybylak, A.; Perez Lorenzo, L. J.; Oberreit, D.; de la Mora, J. F. Cluster activation studies with a diffusive condensation particle counter: Effect of chemical composition. *J. Aerosol Sci.* **2021**, 105917.
72. Wang, X.; Ma, N.; Lei, T.; Größ, J.; Li, G.; Liu, F.; Meusel, H.; Mikhailov, E.; Wiedensohler, A.; Su, H. Effective density and hygroscopicity of protein particles generated with spray-drying process. *J. Aerosol Sci.* **2019,** *137*, 105441.
73. Bornschein, R. E.; Niu, S.; Eschweiler, J.; Ruotolo, B. T. Ion Mobility-Mass Spectrometry Reveals Highly-Compact Intermediates in the Collision Induced Dissociation of Charge-Reduced Protein Complexes. *J. Amer. Soc. Mass Spectrom.* **2016,** *27* (1), 41-49.